the Electromagnetics Branch of the Bureau of Radiological Health, Rockville, MD. His current research interests include the development of techniques for determining the fields inside biological bodies that are exposed to electromagnetic radiation and the development of better and safer methods for using RF and microwave energy.

Dr. Schaubert has been a member of the Technical Review Committee for the Joint Services Electronics Program and of several *ad hoc* panels. He is a member of Tau Beta Pi and Eta Kappa Nu and is currently chairman of the Antennas and Propagation Society Membership Committee.

Frederick G. Farrar (M'80) graduated from Stevens Institute of Technology, Hoboken, NJ, in 1972 with a B.S. degree in physics.

Since 1972 he has been a member of the Microwave Branch of the Advanced Research Laboratory at Harry Diamond Laboratories, U.S. Army ERADCOM, Adelphi, MD.

Current Distribution and Input Impedance of Printed Dipoles

INAM E. RANA AND NICOLAOS G. ALEXOPOULOS, MEMBER, IEEE

Abstract—**Printed dipole antennas find increasing use in microwave as well as far infrared frequencies. The current distribution, input impedance, and radiation pattern are computed for wire antennas printed on a dielectric substrate. The current distribution is obtained by solving Pocklington's equation by moment methods. The Green's function pertinent to the problem involves improper Sommerfeld-type integrals. These integrals are computed by a real-axis integration technique which involves analytical and numerical steps. The effect of surface modes is carefully taken into account.**

I. INTRODUCTION

PRINTED CIRCUIT antennas find increasing use in microwave frequencies as well as in the far infrared where planar-integrated monolithic circuits is the ultimate goal. In the microwave regime these antennas are popular due to their inherent advantages such as conformality to a given surface, low cost, negligible volume, reproducibility, etc. In the submillimeter regime such antennas find use as an integral part of far infrared detectors. The analysis of printed antennas involves Sommerfeld-type integrals which are difficult to deal with when the source and field points are on the substrate, as is the case when one needs to solve Pocklington's equation for the printed antenna current distribution. For this reason the existing analytical techniques to study such antennas, as for example the microstrip patch element in microwave frequencies [1]-[5] or the printed dipole in the microwave regime [6], [7] as well as in the far infared [8], [9], are more of an empirical nature, and they do not provide adequate design criteria. In addition, heretofore published techniques do not account for the effect of the dielectric substrate on the antenna characteristics such as input and mutual impedance. Although for microwave printed antennas the substrate thickness is selected to be much smaller than the wavelength, the fundamental surface wave mode has zero cutoff, and therefore it is always launched in the substrate. Since surface modes decay in the substrate in a manner inversely proportional to the square root of distance (measured from the antenna), even an inefficiently launched surface mode may have an important effect on mutual coupling in a phased-array design. In addition, since the bandwidth of integrated antennas improves with increasing substrate thickness, surface mode effects become significant for the evaluation of a substrate-thickness bandwidth trade-off. On the other hand, in the far infrared, the printed antenna elements which have been tested to date [7], [8] are deposited on substrates which are several wavelengths thick. The presence of several surface modes in these designs provides for phase reversals of the printed dipole current distribution along the dipole length, thus resulting in undesired multiple beam radiation patterns [8].

In this paper a theoretical approach to printed circuit antennas is presented with an application to dipoles printed on a grounded dielectric substrate. Although Pocklington's equation has been developed for printed patch antennas, in this paper attention is confined to printed dipoles with $\hat{x}$ orientation. Previously, the printed dipole problem was treated with an assumed sinusoidal current distribution [10]-[11] or at resonance [12], or as a current distribution derived in the absence of the substrate [13]. The assumption that the printed dipole current distribution is sinusoidal is valid provided that the substrate thickness is exceedingly small compared to the wavelength on the dielectric, or that the printed dipole is of resonant length [11]. In order to solve Pocklington's equation, the appropriate Green's function is obtained by considering a Hertzian dipole printed on the substrate. The resulting Green's function is in terms of Sommerfeld-type integrals [13]-[17], which are very slowly convergent and their derivatives are improper integrals, when the source and field points are on the substrate. An efficient numeric-analytical integration technique has been developed which computes the Green's function for all distances from the source. The solution to Pocklington's equation is then obtained by applying moment methods, yielding in this manner the antenna current distribution, input impedance, substrate thickness, and relative dielectric constant.

Manuscript received November 30, 1979; revised July 23, 1980. This work was supported by the U.S. Army under Contract DAAG 29-79-C-0050.

I. E. Rana is with Suparco, P.O. Box 3209, Karachi 28, Pakistan.

N. G. Alexopoulos is with the Electrical Sciences and Engineering Department, University of California, Los Angeles, CA, 90024.

0018-926X/81/0100-0099$00.75

II. POCKLINGTON'S INTEGRAL EQUATION FOR A PRINTED WIRE

The printed wire dipole considered here is of length L and diameter $2a$, and it is shown in Fig. 1. It is assumed that the radius of the wire is very small as compared to the free-space wavelength ($a \ll \lambda$), and therefore the thin-wire approximation can be used. The current on the wire does not have circumferential symmetry, due to the presence of the grounded substrate. The antenna current distribution may have therefore, in addition to the axial component, a circumferentially nonsymmetric component; yet for a thin wire only the axial component is of significance, e.g., it has been shown [18] that only the axial component is dominant in the determination of the radiation and impedance characteristics. Pocklington's equation for printed wires can be written in the form

$$E_\alpha(x, y, B) = \int_{L_\alpha} I(\alpha') \left\{ k^2 \Pi_\alpha + \frac{\partial^2 \Pi_\alpha}{\partial \alpha^2} + \frac{\partial^2 \Pi_z}{\partial \alpha \partial z} \right\} d\alpha', \quad (1)$$

where $\alpha = x$ or y depending on whether the wire is in the x or y direction, respectively. For this case

$$\Pi_\alpha = \lim_{z \to B} 2K \int_0^\infty J_0(\lambda\rho) e^{-\mu(z-B)} \frac{\lambda d\lambda}{D_e(\lambda)} \quad (2)$$

and

$$\Pi_z = \lim_{z \to B} 2K(1 - \epsilon_r) \cdot \int_0^\infty J_1(\lambda\rho) e^{-\mu(z-B)} \frac{\lambda^2 \Phi_\alpha{}^d \lambda}{D_e(\lambda) D_m(\lambda)}. \quad (3)$$

In the equations above the following parameters need to be defined:

$$D_e(\lambda) = \mu + \mu_e \coth \mu_e B \quad (4)$$

$$D_m(\lambda) = \mu\epsilon_r + \mu_e \tanh \mu_e B, \quad (5)$$

where

$$\mu = [\lambda^2 - k^2]^{1/2}, \qquad \mu_e = [\lambda^2 - \epsilon_r k^2]^{1/2},$$

$$K = -\frac{j}{4\pi\epsilon_0 \omega},$$

$$\rho = [(x - x')^2 + (y - y')^2]^{1/2},$$

and $\Phi_x = \cos\phi$ while $\Phi_y = \sin\phi$. In addition it must be mentioned that in order to obtain the Hertz potentials given by (2) and (3), the canonical problem of a horizontal Hertzian dipole at $z = B$ is solved with a dipole moment p_x. The time dependence $e^{-j\omega t}$ is omitted throughout the paper.

By considering henceforth the printed wire along the x direction, since the wire is unloaded at the ends, the unknown antenna current distribution $I(x')$ must satisfy the end boundary conditions

$$I(0) = I(L) = 0. \quad (6)$$

In order to solve (1) for the antenna current $I(\alpha')$, the method

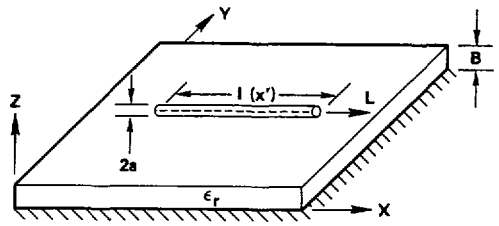

Fig. 1. Printed wire dipole geometry.

of moments is used. Accordingly, the wire is divided into N equal segments. As it is usually, the proper choice of current expansion functions must be made. Sinusoidal expansion functions are employed because they offer many advantages, such as 1) the boundary conditions (6) for the antenna current $I(\alpha')$ are automatically satisfied, 2) a closed-form expression for the fields is obtained, and as will be shown later, and 3) the improperness in the Green's function integrals is removed as $z \to B$. The form of the ith expansion function centered about x_i is simply

$$I(x') = \begin{cases} I_i \left[\dfrac{\sin k(d - |x' - x_i|)}{\sin kd} \right], & |x - x_i| \leqslant d \\ 0, & \text{otherwise,} \end{cases} \quad (7)$$

where d is the length of each segment given by $d = L/N$. By substituting the $N - 1$ term current expansion series into (1), and by making use of the identity $(\partial/\partial_x) = -(\partial/\partial_{x'})$, it can be shown that the x component of the electric field E is given at any point (x, y, B) on the substrate by

$$E_x(x, y, B) = \frac{k}{\sin kd} \sum_{i=2}^{N} I_x \left[\Pi_x|_{x_{i-1}} + \Pi_x|_{x_{i+1}} - 2\cos kd \Pi_x|_{x_i} + 2\cos kd \Pi|_{x_i} - \Pi|_{x_{i-1}} - \Pi|_{x_{i+1}} + k \left[\int_{x_{i-1}}^{x_i} \Pi\, dx' \sin k(x' - x_{i-1}) + \int_{x_i}^{x_{i+1}} \Pi\, dx' \sin k(x_{i+1} - x') \right] \right],$$

where Π_x is given by (2) and

$$\Pi = 2(\epsilon_r - 1)K \lim_{z \to B} \int_0^\infty J_0(\lambda\rho) \cdot e^{-\mu(z-B)} \frac{\lambda\mu\, d\lambda}{D_e(\lambda) \cdot D_m(\lambda)}$$

with

$$\rho = \sqrt{(x - x')^2 + y^2}.$$

Note that (8) does not involve derivatives of Π_x and Π_z. These

derivatives yield improper integrals for $z = B$. Furthermore, the expression for E_x is in closed form, as it involves integrals which are convergent in nature.

For numerical convergence, sinusoidal functions have also been chosen as testing functions. Therefore each side of (8) is multiplied by the testing functions given by (7), with the subscript i replaced by j and the variable x' by x. The integration with respect to x reduces the problem to the matrix form

$$[V] = [I][Z],$$

where I is related to the currents on the subsections and V to the electromagnetic excitation column. Depending upon the feeding point, the corresponding excitation voltage is set to unity in the excitation column.

Matrix inversion is a simple process for high-speed computers, and hence the current distribution can be determined once a well-conditioned impedance matrix $[Z]$ is obtained. The ease and speed of evaluation of the matrix elements is of considerable importance. Evaluation of the matrix elements involves calculation of the following integrals:

$$I_1 = \int_{x_{j-1}}^{x_j} \Pi_x \sin [k(x - x_{j-1})]\, dx + \int_{x_j}^{x_{j+1}} \Pi_x \sin [k(x_{j+1} - x)]\, dx$$

and

$$I_2 = \int_{x_{j-1}}^{x_j} \sin [k(x - x_{j-1})]\, dx \cdot \left[\int_{x_{i+1}}^{x_i} \Pi \sin [k(x' - x_{i-1})]\, dx' + \int_{x_i}^{x_{i+1}} \Pi \sin [k(x_{i+1} - x')]\, dx' \right] + \int_{x_j}^{x_{j+1}} \sin [k(x_{j+1} - x)]\, dx \cdot \left[\int_{x_{i-1}}^{x_i} \Pi \sin k(x' - x_{i-1})\, dx' + \int_{x_i}^{x_{i+1}} \Pi \sin [k(x_{i+1} - x')]\, dx' \right].$$

The double integration with respect to x and x' is performed very efficiently by a numerical technique which makes use of the overlapping nature of the Green's function and removes redundancy in the calculation of the integrand. The integrals (2) and (9) are of the Sommerfeld-type; they require special treatment which is described in the next section.

III. EVALUATION OF THE SOMMERFELD-TYPE INTEGRALS

The Sommerfeld-type integrals given by (2) and (9) contain the two radicals given by μ and μ_e which are double-valued functions of the complex variable λ. However, the sign of the radical represented by μ_e does not affect the single-valuedness of the integrands since the terms involving μ_e are even functions of λ. This imples then that only the branch points contributed by μ need be considered. In order that the integrals represent a proper field solution, the integrand must be single-valued all along the path of integration. This is accomplished by drawing branch cuts through the branch points $\lambda = \pm k$. The choice of the branch cuts is arbitrary as far as single-valuedness is concerned; however, the convergence of the integrals is another matter. The convergence of the integrals and outgoing wave propagating character require Re $\lambda > 0$ and Im $\lambda < 0$, respectively. The choice of the branch cuts and the path of integration are shown in Fig. 2.

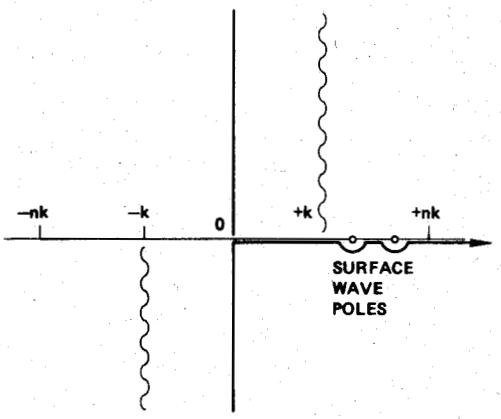

Fig. 2. Path of integration.

A numerical integration of the integrals given by (2) and (9) has been performed by real-axis integration over the $0 \leqslant \lambda < \infty$ interval. The convergence of these integrals can be enhanced due to the presence of the factor $\exp(-\mu(z - B))$ in the integrands. When the antenna is printed on the substrate $z = B$, this factor tends to unity. For this case the integrals given by (2) and (9) are proper but very slowly convergent. The numerical integratioin is carried out by employing Simpson's rule up to $\lambda = Q$, where Q is chosen so that the relation $\coth(BQ) \cong 1.0$ is satisfied. When $\lambda > Q$ the integral can be evaluated analytically. The integration over the range $0 \leqslant \lambda < \infty$ is divided into the following subintervals.

1) $0 < \lambda < k$: Integration over this interval is performed numerically. The integrals contribute to the radiation resistance and to the reactive part of the input impedance.

2) $k < \lambda < (\epsilon_r)^{1/2} k$: The integrands have poles in this interval. The poles correspond to the surface wave modes excited by the antenna. The number of modes excited depends upon the thickness B of the substrate, its dielectric constant ϵ_r, and the frequency of operation. The modes are zeros of the factors

$$D_e(\lambda) = \mu + \mu_e \coth \mu_e B, \qquad \text{TE modes}$$

$$D_m(\lambda) = \epsilon_r \mu + \mu_e \tanh \mu_e B, \qquad \text{TM modes.}$$

By using the singularity extraction technique, the integral can be written as

$$\int_k^{nk} \frac{f(\lambda)}{(\lambda - \lambda_0)}\, d\lambda = \int_k^{nk} \frac{f(\lambda) - f(\lambda_0)}{(\lambda - \lambda_0)}\, d\lambda + \int_k^{nk} \frac{f(\lambda_0)}{(\lambda - \lambda_0)}\, d\lambda, \tag{10}$$

where $n = (\epsilon_r)^{1/2}$ is the index of refraction of the substrate. The first integral on the right-hand side of (10) can be evaluated numerically, while the second integral can be integrated analytically. This technique can be extended depending on the number of modes.

3) $nk < \lambda < Q$: Numerical integration is again invoked here. The choice of the number Q depends mainly on the thickness of the substrate B and its dielectric constant ϵ_r. The factor Q is such that it satisfies

$$\coth (B\sqrt{\lambda^2 - n^2k^2}) \cong 1.0, \qquad \text{for all } \lambda > Q. \tag{11}$$

4) $Q < \lambda < \infty$: The special nature of the integrand is involved in this interval. The use of (11) simplifies the integrand to a form which involves the radicals μ, μ_e. Since $\lambda > k$ and nk, after application of the binomial series expansion to these radicals the tail part of the integrals can be written as

$$2\int_Q^\infty \frac{J_0(\lambda\rho)}{\mu + \mu_e}\, d\lambda = \int_Q^\infty d\lambda J_0(\lambda\rho)\left[1 + \frac{XL}{\lambda^2} + \frac{XT}{\lambda^4} + \frac{XC}{\lambda^6} + \cdots\right],$$

where $XL = Lk^2$, $XT = (L^2 + M)k^4$, $XC = (L^3 + 2LM + N)k^6$ with $L = (\epsilon_r + 1)/4$, $M = (\epsilon_r{}^2 + 1)/16$, and $N = (\epsilon_r{}^3 + 1)/32$. Thus the integrand has been reduced to a highly convergent series, and therefore term by term integration can be performed analytically.

IV. INPUT IMPEDANCE AND RADIATION PATTERN

The problem for the current distribution of the printed dipole was formulated in the previous section. The solution described uses sinusoidal subsection currents and Galerkin's method, while the dipole is assumed to be excited by an idealized source, the delta gap generator. In air it has been found that the input impedance is not critically dependent upon the excitation gap length as long as it is $< 0.1\ \lambda_0$. Therefore, neglecting the effect of the incoming excitation line, the input impedance for a small gap between the input terminals will be as seen by the delta gap generator. In the computations of current distribution, the circumferential variation of the antenna has been neglected. This is due to the fact that whatever device is used to measure the input impedance, it is insensitive to the circumferential variation of the current, provided the wire is very thin. The input impedance of the printed wire dipoles for a 1.0-V input excitation is given by

$$Z_{\text{in}} = 1.0/I_{\text{in}},$$

where I_{in} is the current at the input terminals of the antenna, obtained from knowledge of the current distribution.

In order to compute the radiation pattern, the stationary phase method is used [10]. The far-zone electric field components for $\theta < 90^\circ$ are given by

$$E_\theta(\theta, \phi) = 2k^2 \Pi_\theta \tag{13}$$

and

$$E_\phi(\theta, \phi) = 2k^2 \Pi_\phi, \tag{14}$$

where Π_θ and Π_ϕ are expressed as

$$\Pi_\theta = K\frac{e^{jkr}}{r} \cdot \left[\frac{e^{-jkB\cos\theta}}{D_e(\theta, \phi)}\cos\theta + \frac{n^2 - 1}{n^2}\,\frac{\tan\theta\sin\theta}{D_m(\theta, \phi)}\cos\phi\right] I_x \tag{15}$$

and

$$\Pi_\phi = K\frac{e^{jkr}}{r}\,\frac{e^{-jkB\cos\theta}}{D_e(\theta, \phi)}\sin\phi I_x.$$

The parameter I_x is in this case

$$I_x = \int_{L_x} I(x')e^{-jkx\sin\theta\cos\phi}\, dx', \tag{17}$$

and it is computed numerically.

V. NUMERICAL RESULTS

Based on the previously developed analysis numerical computations have been performed for a very thin wire dipole with a typically chosen radius of $a = 0.0001\ \lambda_0$. The dipoles are center fed by an in-phase delta gap generator, and all pertinent dimensions are normalized to the free-space wavelength λ_0.

The computations have been performed so that the effect of one- or two-surface modes to the antenna current distribution is clarified. This is accomplished by considering a quartz-like substrate ($\epsilon_r \cong 3.25$) [11] for a single-surface mode and alumina-like substrate ($\epsilon_r \cong 8.5$) for the two-surface modes. Fig. 3 shows the Re [I] and Im [I] components of the dipoles current distribution for a dipole length of $0.5\ \lambda_0$, substrate thickness of $B = 0.1016\ \lambda_0$, and $\epsilon_r = 3.25$. The current distribution presents a dip at the feeding point because of the fact that the presence of the substrate increases the effective electrical length of the dipole [11]. When $\epsilon_r = 1.0$ (air substrate) the current distribution is about ten times as large in magnitude over the printed dipole, as indicated by a comparison between Fig. 3 and 4. An increase in the substrate thickness to $B = 0.127\ \lambda_0$ is seen to change the current level but to have a minor influence on the current distribution (see Fig. 5). This indicates that the input impedance is sensitive to changes in B. A substantial increase in B or a moderate increase in B to $0.15\ \lambda_0$, and a change of the substrate dielectric constant to $\epsilon_r = 8.5$, allows two propagating surface wave modes. The current distribution for this latter case is shown in Fig. 6. The figure indicates that both Re [I] and Im [I] undergo sign changes, and more importantly that there is a substantial increase in the effective electrical length of the dipole.

It can be inferred from the above discussion that the impedance level of the printed dipole is higher than the dipole, over the grounded plane. This higher impedance level is attributed to the fact that the printed dipole radiates power as space waves and launches a surface wave in the dielectric surface guide. However, this surface wave contributes only to the real part of the input impedance. The higher order non-

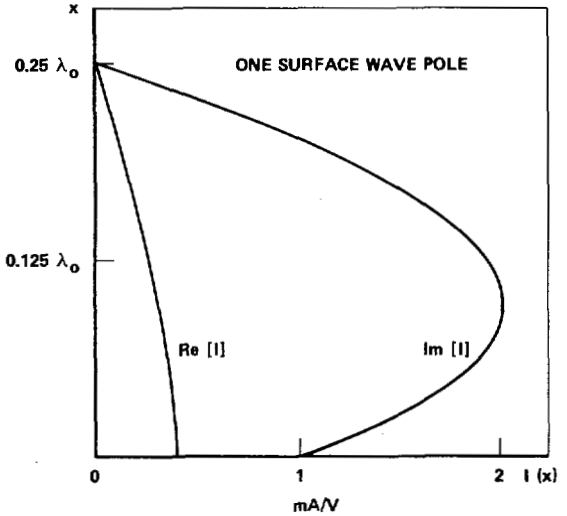

Fig. 3. Current distribution on a printed wire dipole Re[I] and Im[I] versus x (in λ_0), ($B = 0.1016\ \lambda_0$, $\epsilon_r = 3.25$, $a = 0.00005\ \lambda_0$).

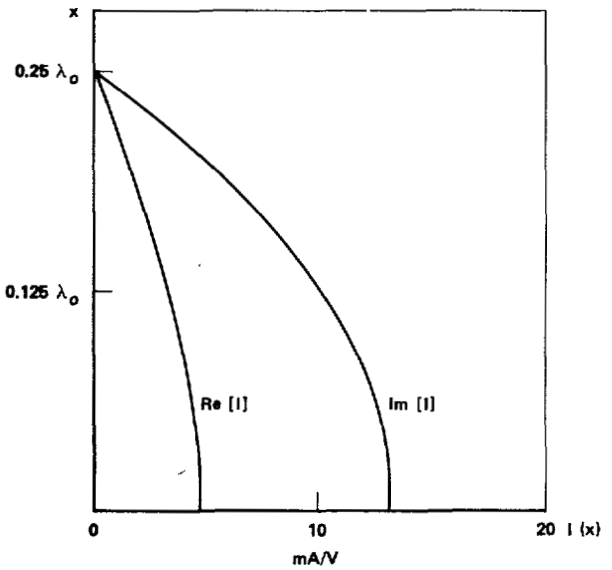

Fig. 4. Current distribution on a printed wire dipole Re[I] and Im[I] versus x (in λ_0), ($B = 0.1016\ \lambda_0$, $\epsilon_r = 1.0$, $a = 0.00005\ \lambda_0$).

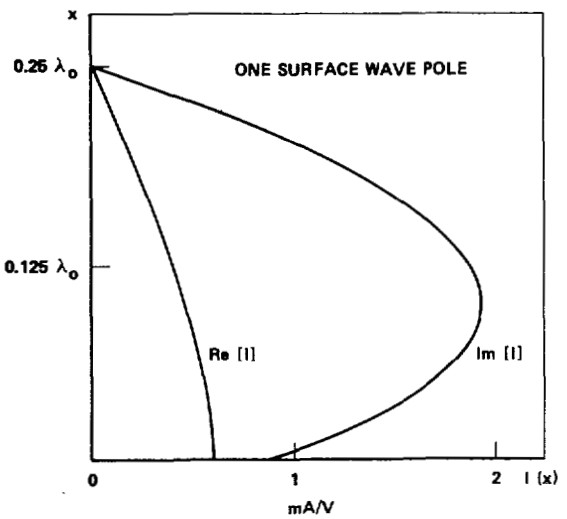

Fig. 5. Current distribution on a printed wire dipole Re[I] and Im[I] versus x (in λ_0), ($B = 0.127\ \lambda_0$, $\epsilon_r = 3.25$, $a = 0.00005\ \lambda_0$).

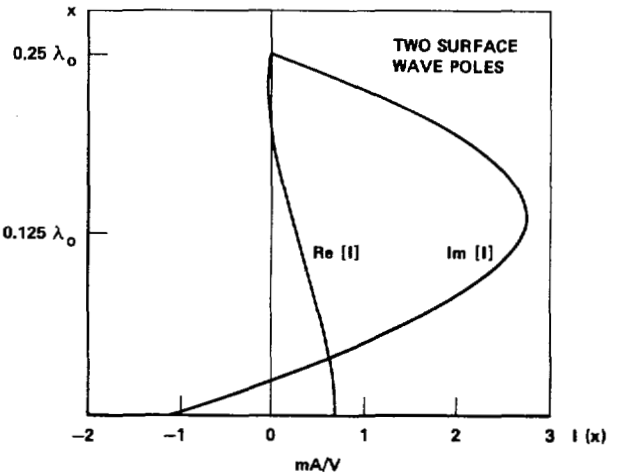

Fig. 6. Current distribution on a printed wire dipole Re[I] and Im[I] versus x (in λ_0), ($B = 0.15\ \lambda_0$, $\epsilon_r = 8.5$, $a = 0.00005\ \lambda_0$).

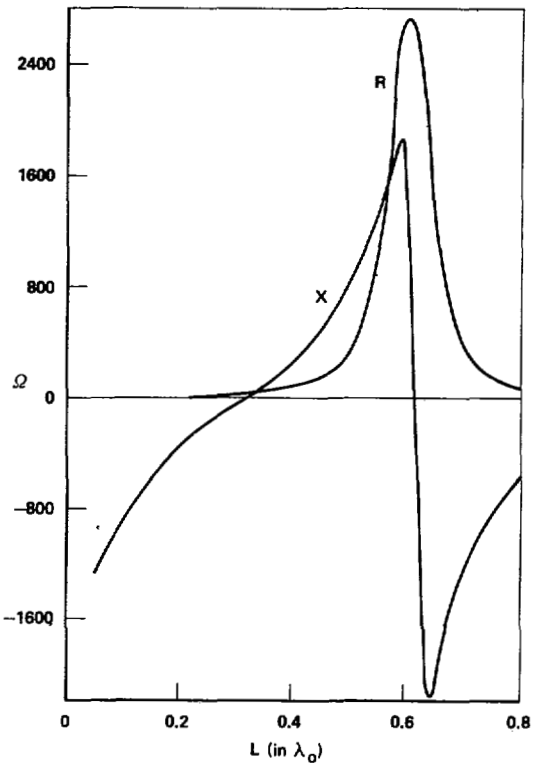

Fig. 7. Input impedance of a printed wire dipole versus L (in λ_0), ($B = 0.1016\ \lambda_0$, $\epsilon_r = 3.25$, $a = 0.00005\ \lambda_0$).

propagating modes contribute to the reactive part of the input impedance. Figs. 7–9 show the input impedance of the printed dipole versus its length L, for the different substrate thicknesses and dielectric constants. Comparison of the resonant length L_r and the input impedance Z_{in} for all the above-mentioned cases is given in Table I. The real part of the Z_{in} is the sum of two terms, namely, the radiation resistance and the surface wave launching resistance. By increasing the substrate thickness from 0.1016 to 0.127 λ_0, the resonant impedance increases from 34.5 to 60 Ω. This increase in value of the resonant input impedance is essentially due to the fact that an increase in B (still referring to a single surface wave mode) increases both the surface wave launching as well as radiation efficiencies.

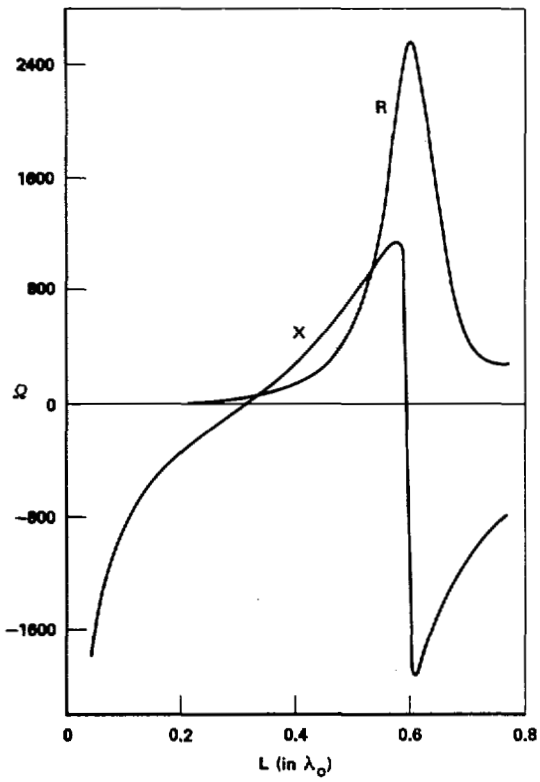

Fig. 8. Input impedance versus antenna length L (in λ_0), (B = 0.127 λ_0, ϵ_r = 3.25, a = 0.00005 λ_0).

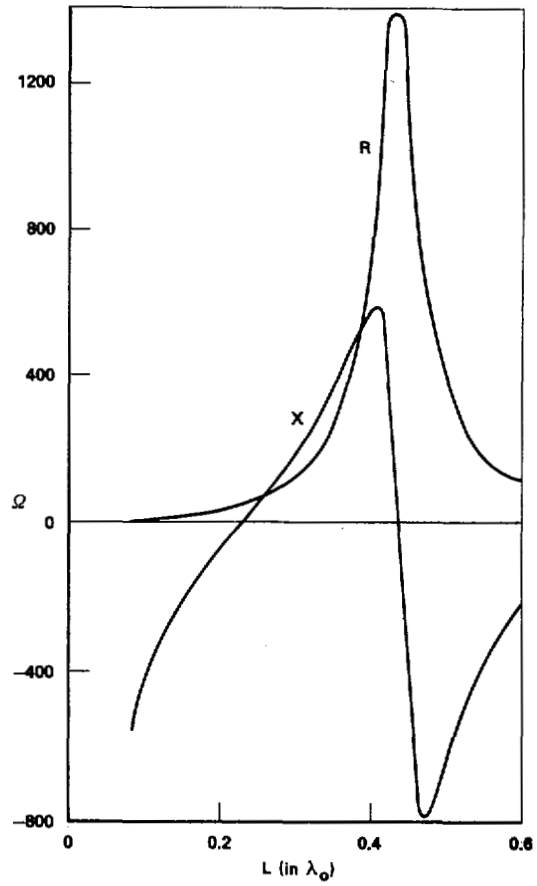

Fig. 9. Input impedance of a printed wire dipole versus L (in λ_0), (B = 0.15 λ_0), ϵ_r = 8.5, a = 0.000025 λ_0).

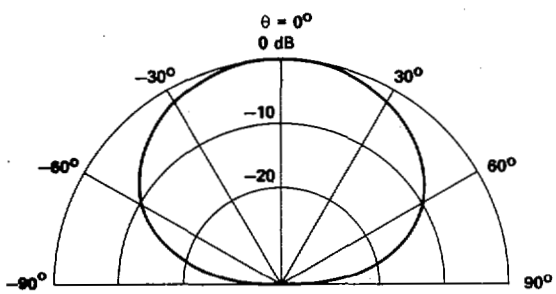

Fig. 10. E-plane radiation plot of a printed wire dipole (L = 0.333 λ_0, ϵ_r = 3.25).

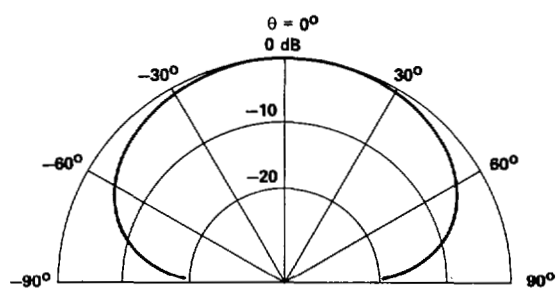

Fig. 11. H-plane radiation plot of a printed wire dipole (L = 0.333 λ_0, B = 0.1016 λ_0, ϵ_r = 3.25).

TABLE I
PRINTED DIPOLE PARAMETERS FOR DIFFERENT VALUES OF B AND ϵ_r

Number of modes	ϵ_r	B	L_r	Z_{in} (resonant)	Z_{in} (for L = 0.5 λ_0)
1	3.25	0.1016 λ_0	0.317 λ_0	34.5 + j0 Ω	330 − j880 Ω
1	3.25	0.127 λ_0	0.315 λ_0	60.0 + j0 Ω	535 − j788 Ω
2	8.50	0.150 λ_0	0.230 λ_0	50.0 + j0 Ω	418 + j664 Ω

The two propagating surface wave modes also effect the impedance characteristics of the printed dipole. The increased dielectric constant ($\epsilon_r = 8.5$) reduces the radiation resistance (efficiency) of the printed dipole [11].

Lastly, E- and H-plane radiation patterns of the printed dipole are shown in Figs. 10 and 11. Near the air dielectric interface, i.e., $\theta = \pm 90^\circ$, the radiation plots are not exact since the stationary phase method used in the development of the formula for the radiated fields is not valid when $\theta = \pm 90^\circ$.

VIII. CONCLUSION

The radiation characteristics of wires printed on a grounded substrate have been investigated. The current distribution has been obtained by employing moment methods to solve Pocklington's equation. The improperness of the Sommerfeld-type integrals, when the field and source points are on the substrate, has been circumvented by employing a correct limiting process and sinusoidal expansion as well as testing functions for the numerical integration along the real axis. In addition, the effect of surface wave modes on the current distribution and input impedance was determined.

REFERENCES

[1] R. E. Munson, "Conformal microstrip antennas and microstrip phased arrays," *IEEE Trans. Antennas Propagat.*, vol. AP-22, pp. 74–78, Jan. 1974.

[2] J. E. Howell, "Microstrip antennas," *IEEE Trans. Antennas Propagat.*, vol. AP-23, pp. 90–93, Jan. 1975.

[3] A. G. Derneryd, "A theoretical investigation of the rectangular microstrip antenna element," *IEEE Trans. Antennas Propagat.*, vol. AP-26, pp. 532–535, July 1978.

[4] Y. T. Lo, D. Solomon, and W. F. Richards, "Theory and experiment on microstrip antennas," *IEEE Trans. Antennas Propagat.*, vol. AP-27, pp. 137–145, Mar. 1979.

[5] P. K. Agarwal and M. C. Bailey, "An analysis technique for microstrip antennas," *IEEE Trans. Antennas Propagat.*, vol. AP-25, pp. 756–759, Nov. 1977.

[6] D. A. Huebner, "An electrically small microstrip dipole planar array," in *Proc. Workshop on Printed Circuit Antenna Technol.*, Las Cruces, NM, Oct. 1979, pp. 17.1–17.16.

[7] H. G. Oltman and D. A. Huebner, "Electromagnetically coupled microstrip dipoles, *IEEE Trans. Antennas Propagat.*, vol. AP-29, pp. 152–158, Jan. 1981, this issue.

[8] D. B. Rutledge, S. E. Schwarz, and A. T. Adams, "Infrared and submillimeter antennas," *Infrared Phys.*, vol. 18, pp. 713–729, Dec. 1978.

[9] K. Mizuno, Y. Daiku, and S. Ono, "Design of printed resonant antennas for monolithic-diode detectors," *IEEE Trans. Microwave Theory Tech.*, vol. MTT-25, pp. 470–476, June 1977.

[10] G. N. Tsandoulas, "Excitation of a grounded dielectric slab by a horizontal dipole," *IEEE Trans. Antennas Propagat.*, vol. AP-17, pp. 156–161, Mar. 1969.

[11] N. K. Uzunoglu, N. G. Alexopoulos, and J. G. Fikioris, "Radiation properties of microstrip dipoles," *IEEE Trans. Antennas Propagat.*, vol. AP-27, pp. 853–858, Nov. 1979.

[12] G. Dubost, "Theory and experiments of a broadband short-circuited microstrip dipole at resonance," in *Proc. Workshop on Printed Circuit Antenna Technol.*, Las Cruces, NM, Oct. 17–19, 1979.

[13] A. Sommerfeld, *Partial Differential Equations in Physics*. New York: Academic, 1949, vol. VI.

[14] J. R. Wait, "Characteristics of antennas over lossy earth," in *Antenna Theory, Part 2*. New York: McGraw-Hill, 1969, ch. 23.

[15] P. Parhami, Y. Rahmat-Samii, and R. Mittra, "An efficient approach for evaluating the Sommerfeld integrals encountered in the current element radiating over lossy ground," *IEEE Trans. Antennas Propagat.*, vol. AP-28, pp. 100–104, Jan. 1980.

[16] J. A. Kong, "Electromagnetic fields due to dipole antennas over stratified anisotropic media," *Geophys.*, vol. 37, pp. 985–996, Dec. 1972.

[17] G. J. Burke, E. K. Miller, J. N. Brittingham, D. L. Lager, R. J. Lytle, and J. T. Okada, "Computer modeling of antennas near the ground," Lawrence Livermore Lab. Rep. UCID-18626, May 13, 1980.

[18] P. Tulyanthan and P. K. Newman, "The circumferential variation of the axial component of current in closely space thin wire antennas," *IEEE Trans. Antennas Propagat.*, vol. AP-27, Jan. 1979.

Inam E. Rana was born December 14, 1949, in Pasrar, Pakistan. He obtained the B.S.E.E. degree in 1973 from the University of Engineering and Technology Lahore, Pakistan. He also obtained the M.S.E.E. and Ph.D. degrees from the University of California, Los Angeles, CA in 1977 and 1979, respectively.

He is currently working for Suparco in Karachi, Pakistan. His current research interests are in the area of electromagnetic theory with applications to integrated microwave circuits and microstrip antennas.

Nicolaos G. Alexopoulos (S'68–M'69) was born in Athens, Greece, March 30, 1942. He obtained the B.S.E.E. degree in 1964, the M.S.E.E. degree in 1967 and the Ph.D. degree in 1968 at the University of Michigan, Ann Arbor, MI.

Since the Fall 1969 he has been with the Electrical Sciences and Engineering Department, University of California, Los Angeles. His research interests are in the area of applied electromagnetic theory with current emphasis on integrated microwave circuits, antennas, and scattering. He is the author of over 40 publications in scientific literature.